Available online at www.eccomasproceedia.org
Eccomas Proceedia COMPDYN (2025) 2559-2570

ECCOMAS
Proceedia

COMPDYN 2025
10th ECCOMAS Thematic Conference on
Computational Methods in Structural Dynamics and Earthquake Engineering
M. Papadrakakis, M. Fragiadakis (eds.)
Rhodes Island, Greece, 15-18 June 2025

THREE-DIMENSIONAL EARTHQUAKE-INDUCED COLLAPSE SIMULATION OF STEEL BUILDINGS WITH A NEW BEAM-COLUMN ELEMENT WITH SELECTIVE GRADIENT-INELASTICITY

D.I. Heredia Rosa[1], A. de Castro e Sousa[2], D. Lignos[3]

[1] Postdoctoral Researcher, School of Architecture, Civil and Environmental Engineering, École Polytechnique Fédérale de Lausanne (EPFL), Station 18, Lausanne 1015, Switzerland
e-mail: diego.herediarosa@epfl.ch

[2] Scientist, School of Architecture, Civil and Environmental Engineering, École Polytechnique Fédérale de Lausanne (EPFL), Station 18, Lausanne 1015, Switzerland
e-mail: albano.sousa@epfl.ch

[3] Professor and Chair, School of Architecture, Civil and Environmental Engineering, École Polytechnique Fédérale de Lausanne (EPFL), Station 18, Lausanne 1015, Switzerland
e-mail: dimitrios.lignos@epfl.ch

Abstract. *This paper demonstrates new methodological developments in 3-dimensional (3-D) nonlinear collapse simulations of steel buildings under earthquake shaking. In particular, a novel modeling approach is proposed, including a recently developed 3-D beam-column element with selective gradient-inelasticity. The proposed gradient-inelastic formulation ensures mesh-convergent results in the presence of a material law exhibiting softening. The formulation features a newly developed multiaxial constitutive relation with softening that allows for explicit consideration of both cyclic hardening typically observed in steel materials, and the cyclic strength and stiffness deterioration of beam-columns due to inelastic local buckling. The overall modeling approach is validated by both (a) member-level and (b) system-level collapse simulations. The former relies on comparisons with prior available tests on steel beam-columns with hollow square sections (HSS) and wide flange sections. System-level validations feature a full-scale four-story steel frame building that was tested through collapse on the E-Defense shake table in Japan. The 3-D simulation results with the proposed element formulation provide valuable insights into the fundamental mechanisms governing the structural response up to collapse and the primary differences with predictions from 2-D simulations.*

Keywords: Earthquake-induced collapse, steel frame structures, 3-D fiber-based beam-column element, gradient-based mechanics

ISSN:2623-3347
Peer-review under responsibility of the organizing committee of COMPDYN 2025.
doi: 10.7712/120125.12590.24868

1 INTRODUCTION

Accurate prediction of the structural response under seismic loading is a key objective in performance-based earthquake engineering [1, 2]. In the case of steel structures, predictive models should capture material nonlinearities and the deterioration of strength and stiffness due to geometric nonlinearities such as local buckling [3]. Traditional modeling approaches rely on two-dimensional (2-D) simulations using point hinge elements for flexure [4, 5]. However, these models cannot capture the spread on plasticity along the member length, the interaction of different loading modes (axial load, shear, and bi-axial bending), as well as axial shortening that may be critical at large deformations associated with structural collapse.

Fiber-based beam-column elements allow to overcome some of these limitations [6, 7]. However, such elements are unable to explicitly represent the effects of nonlinear geometric instabilities such as local buckling. This necessitates the use of an effective multiaxial material law with softening. In the presence of softening, strain localization and mesh divergence occur within a fiber-based beam-column element, thereby leading to non-objective numerical results. Specifically, in force-based beam-column elements, this localization concentrates at a single integration section along the element length, causing the response to diverge with an increase in the number of integration sections [6, 8, 9].

To address these challenges, this paper presents a newly proposed three-dimensional (3-D) beam-column element formulation with selective gradient inelasticity along with a new multiaxial material law with softening. This approach ensures a mesh-convergent representation of local nonlinear geometric instabilities. The model is validated to test data from prior component and system-level experiments with emphasis at earthquake-induced collapse.

2 OVERVIEW OF THE PROPOSED MODELING APPROACH

This section presents an overview of the proposed modeling approach, which combines a beam-column element with selective gradient-inelasticity and a multiaxial material law with softening. The gradient-inelastic element is designed to mitigate strain localization and mesh-divergence. The multiaxial material law accounts for both isotropic and kinematic hardening, as well as softening and subsequent recovery, to represent the local buckling deformations within steel members subject to inelastic cyclic loading.

2.1 Multiaxial material law with softening

This section summarizes the key features of the multiaxial material law with softening proposed in [10, 11]. The present work idealizes steel members (specifically, wide-flange and hollow square HSS sections) as an assembly of different plates with appropriate boundary conditions. In this section, the main load paths of the proposed multiaxial material law formulation, namely the hardening path, the softening path, and the recovery path, are discussed. For more details, the reader is referred to the aforementioned publications.

As shown in Figures 1 and 2, the yield criterion consists of two distinct ellipsoid surfaces

that correspond to the stress state, i.e. tensile or compressive, based on the sign of the first invariant of the stress tensor ($I_1 = \sigma_{ii}$). During post-yield hardening, both yield surfaces are the von Mises yield surface (see Figure 1a). It is worth noting that the yield criterion remains continuous and differentiable at every point on its surface, as the two ellipsoid surfaces share the same radius in the π-plane (i.e., $I_1 = 0$), as depicted in Figures 1 and 2.

Using the definition of the multiaxial fiber stress state [10], the mathematical formulation of the chosen yield criterion is given by Equation 1. This formulation of the yield criterion solely involves the stress and strain components relevant to multiaxial fiber-based beam-column elements, specifically the axial and two in-plane shear components [12, 13].

$$\phi = \begin{cases} \phi^{Tens} : \frac{3}{2}\boldsymbol{\xi}^T \boldsymbol{P} \boldsymbol{\xi} + \chi_{1t} \left(\boldsymbol{p}^T \boldsymbol{\sigma}\right)^2 - \sigma_y^2 \leq 0 & \text{for} \quad I_1 \geq 0 \\ \phi^{Comp} : \frac{3}{2}\boldsymbol{\xi}^T \boldsymbol{P} \boldsymbol{\xi} + \chi_{1c} \left(\boldsymbol{p}^T \boldsymbol{\sigma}\right)^2 - \sigma_y^2 \leq 0 & \text{for} \quad I_1 \leq 0 \end{cases} \tag{1}$$

where ϕ^{Tens} and ϕ^{Comp} denote the yield surfaces under tensile and compressive stresses, respectively, $\boldsymbol{\xi} = \boldsymbol{\sigma} - \boldsymbol{\alpha}$ denotes the relative stress ($\boldsymbol{\alpha}$ is the backstress component), σ_y denotes the yield stress and χ_{1t} and χ_{1c} the parameters guiding the ellipsoid yield surface evolution in the softening and recovery paths, under tensile and compressive stresses, respectively.

It is assumed that the strain vector $\boldsymbol{\varepsilon}$ can be decomposed into the sum of three strain components, as shown in Equation 2

$$\boldsymbol{\varepsilon} = \boldsymbol{\varepsilon}^e + \boldsymbol{\varepsilon}^p + \boldsymbol{\varepsilon}^{pb} \tag{2}$$

where $\boldsymbol{\varepsilon}^e$ denotes the elastic strain vector, $\boldsymbol{\varepsilon}^p$ the plastic strain vector and $\boldsymbol{\varepsilon}^{pb}$ the post buckling strain vector which represents the softening deformations. With this strain decomposition, the stress-strain relation is given by

$$\boldsymbol{\sigma} = \boldsymbol{C}(d) \left(\boldsymbol{\varepsilon} - \boldsymbol{\varepsilon}^p - \boldsymbol{\varepsilon}^{pb}\right) \tag{3}$$

where d is a function of a damage variable d introduced to control the reduction of the elastic tangent modulus due to local buckling deformations within the steel plate.

The equations governing the post-yield hardening response in tension and compression are provided in previous work [14, 10], and are therefore omitted here for brevity.

The softening path represents the evolution of local buckling deformations within a steel member. During softening, the yield surface radius parallel to the hydrostatic axis shrinks, while the yield surface center and radius in the π-plane remain constant. According to Equation 1, the reduction in the radius along the hydrostatic axis of the compressive yield surface is achieved by increasing the parameter χ_{1c}. During the softening path, the evolution of χ_{1c}, is informed from appropriate yield line mechanics that have been proposed and validated for each plate type. To meet the tensile surface at a specific stress state following a load reversal from softening, the tensile yield surface shrinks along the hydrostatic axis simultaneously with the compressive surface. The evolution of the yield surface during softening is depicted in Figures 1a to 1c, with Figure 1d illustrating this evolution in a 2D cut of the yield surface.

The recovery path consists in the restoration of local buckling deformations within the steel plate that occurred during the softening path. Figures 2a to 2c depict the yield surface evolution during the recovery path, while Figure 2d describes the yield surface evolution with a 2D cut

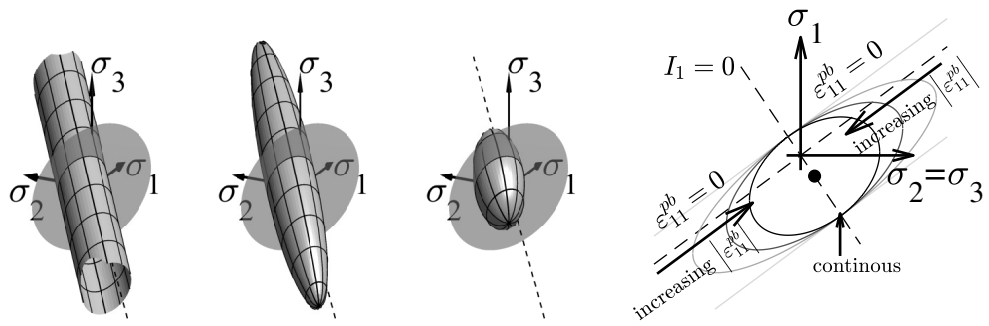

(a) (b) (c) (d)

Figure 1: Yield surface evolution during softening

of the yield surface. The evolution of the yield surface during recovery is governed by three mechanisms: (1) the increase in the radius of the yield surface along the π-plane, (2) the translation of the yield surface center along the π-plane and (3) the increase radius of the tensile and compressive yield surfaces along the hydrostatic axis. From the tensile and compressive yield criteria given in Equation 1, the first two evolution mechanisms require updates to both the yield stress σ_y and the backstress $\boldsymbol{\alpha}$. The third mechanism is realized by decreasing the parameters χ_{1t} and χ_{1c}, which leads to increasingly prolate tensile and compressive yield surfaces. During the recovery path, the evolution of the tensile yield surface is based on third-order Bezier curves [15], which are calibrated based on the results of finite element simulations on steel plates subjected to monotonic loading followed by unloading. Once the evolution rules for σ_y, α, and χ_{1t} are established, a return mapping algorithm is formulated to determine the stress state corresponding to a given input strain vector.

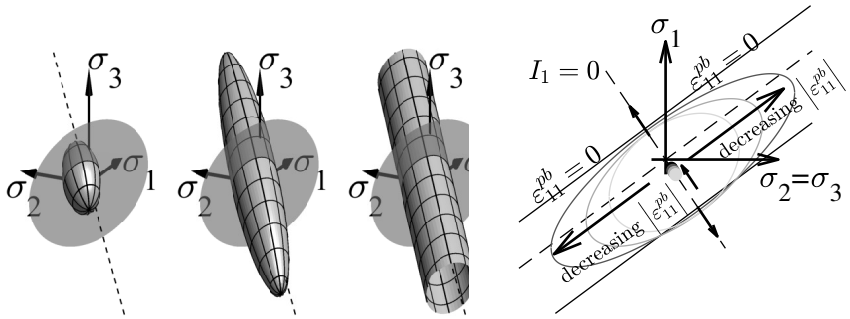

(a) (b) (c) (d)

Figure 2: Yield surface evolution during recovery

When the softening deformations have been fully recovered, χ_{1t} and χ_{1c} are both zero, and both the tensile and compressive yield surfaces consist of the von-Mises yield surface, as shown in Figure 2c. After this point, loading in the hardening path is resumed.

2.2 Fiber-based beam-column element with selective gradient-inelasticity

A gradient-inelastic formulation is proposed to enrich standard force-based beam-column elements. In the present work, the gradient-inelastic formulation is applied to the increment in

section deformations $\Delta \boldsymbol{e}$. The implicit gradient relation [16] between the increment in macroscopic (i.e., the averaged) section deformations $\Delta \overline{\boldsymbol{e}}$ and the increment in material (i.e., the local) section deformations $\Delta \boldsymbol{e}$ is given by

$$\Delta \overline{\boldsymbol{e}} - \frac{1}{2} l_c^2 \nabla^2 \Delta \overline{\boldsymbol{e}} = \Delta \boldsymbol{e} \tag{4}$$

where l_c is the characteristics length of the problem, which is taken as the local buckling length of the member [3, 17, 18]. Equation 4 can be solved using a second-order finite difference approximation, applied at the various integration sections placed along the element length. For this, two Dirichlet boundary conditions are specified, ensuring that at the element ends, the increment in material section deformations is equal to the increment in macroscopic section deformations. The relationship between the increment in macroscopic section deformations and the increment in material section deformations can be expressed as follows:

$$\Delta \overline{\boldsymbol{e}}_{all} = \boldsymbol{H}^{-1} \cdot \Delta \boldsymbol{e}_{all} \tag{5}$$

where $\Delta \overline{\boldsymbol{e}}_{all}$ and $\Delta \boldsymbol{e}_{all}$ contain the increment in macroscopic and material section deformations, respectively, from every integration section along the element length. The matrix $\boldsymbol{H}$ averages the values between the sections along the element length and, for equally spaced integration points, depends on two parameters, a_c and b_c.

To prevent the results in the pre-peak domain from being influenced by the characteristic length l_c, this work suggests applying the gradient averaging formulation only after the element begins to soften. In contrast, the local formulation should be used during the non-softening response, and thus no averaging should be performed. The transition between the local and gradient-inelastic formulations is controlled by updating the coefficients a_c and b_c in the matrix $\boldsymbol{H}$. In the non-softening phase, $\boldsymbol{H}$ is set to the identity matrix, hence $a_c = 1$ and $b_c = 0$. During the softening phase at the element level, a_c and b_c are updated to the values from the implicit gradient formulation. The switch between these values is achieved by leveraging a smooth exponential function, which is computed using the introduced section strain energy in softening W^{soft}, defined as

$$W_{n+1}^{soft} = \begin{cases} \max\left(\min\left(W_n^{soft} + \Delta W^{unload}, 0\right), W_{tol}^{soft}\right) & \text{if all sections unload elastically} \\ \max\left(\min\left(W_n^{soft} + \Delta W^{soft}, 0\right), W_{tol}^{soft}\right) & \text{else} \end{cases} \tag{6}$$

where ΔW^{soft} and ΔW^{unload} represent the accumulated increments in section strain energy for sections undergoing softening and elastic unloading, respectively, along the element length. The term W_{tol}^{soft} is a small threshold value for section strain energy. The increment in section strain energy for a given section x_l is defined as

$$\Delta W_{sec}\left(x_l\right) = \frac{1}{2} \Delta \boldsymbol{s}\left(x_l\right) \cdot \Delta \boldsymbol{e}\left(x_l\right) \tag{7}$$

According to Equation 6, the section strain energy W^{soft} increases with the increment in section softening strain energy ΔW^{soft} and decreases with the increment in section unloading strain energy ΔW^{unload}. This quantity W^{soft} is then used to define the exponential smooth transition function governing the change between the two sets of coefficients in matrix $\boldsymbol{H}$.

The conventional element state determination for force-based beam-column elements is enhanced with the proposed selective gradient-inelasticity formulation. The resulting procedure, detailed in [19], is applicable to both 2D and 3D force-based beam-column elements. Building on previous studies [20, 21], the present formulation incorporates the macroscopic section deformations in the relationship between element displacements and section deformations, while the material section deformations are used in the section force-displacement relationship.

3 VALIDATION STUDIES

In this section, the proposed modeling approach is integrated into a standard 3-dimensional Timoshenko force-based beam-column element in OpenSees [22]. Simulations at both the member and system levels are conducted, and the results are compared with experimental data.

3.1 Member-level

The proposed modeling approach is used to simulate test specimen C6 from [3], which consists in a 3.9 meters high column with a W24x146 wide flange section. The column is subjected to bidirectional cyclic load protocols and a constant axial load. The developed multiaxial constitutive material formulation discussed in the previous section is used. Model parameters for hardening are taken from [14] for A992 Gr.50 steel, while parameters for softening are computed using the method proposed in [10, 11]. An elastic rotational spring is added at the column base along the strong axis direction to represent the flexibility of the experimental setup [3]. For the gradient formulation, a characteristic length of $l_c = 1.0d$ (where d is the section depth) is chosen, corresponding to the buckling length of test specimen [3]. The integration sections are distributed along the element length using the Simpson quadrature rule [23], ensuring that at least three sections are within the characteristic length.

Figure 3 shows the simulation results from the local ($l_c = 0$) element formulation (Figures 3a and 3c) and the proposed formulation with selective gradient inelasticity using three different integration sections (Figures 3b and 3d) The moment-rotation relation in Figures 3a exhibits mesh divergence due to strain localization, showing a steeper negative slope and accelerated strength deterioration in the softening stage as the number of integration sections along the element length increases. In contrast, Figure 3b demonstrates that as the number of integration sections increases, the moment-rotation relation converges to a consistent solution, with only minor discrepancies due to cumulative effects across loading cycles. The same trend is observed in the axial shortening-rotation response (Figures 3c and 3d).

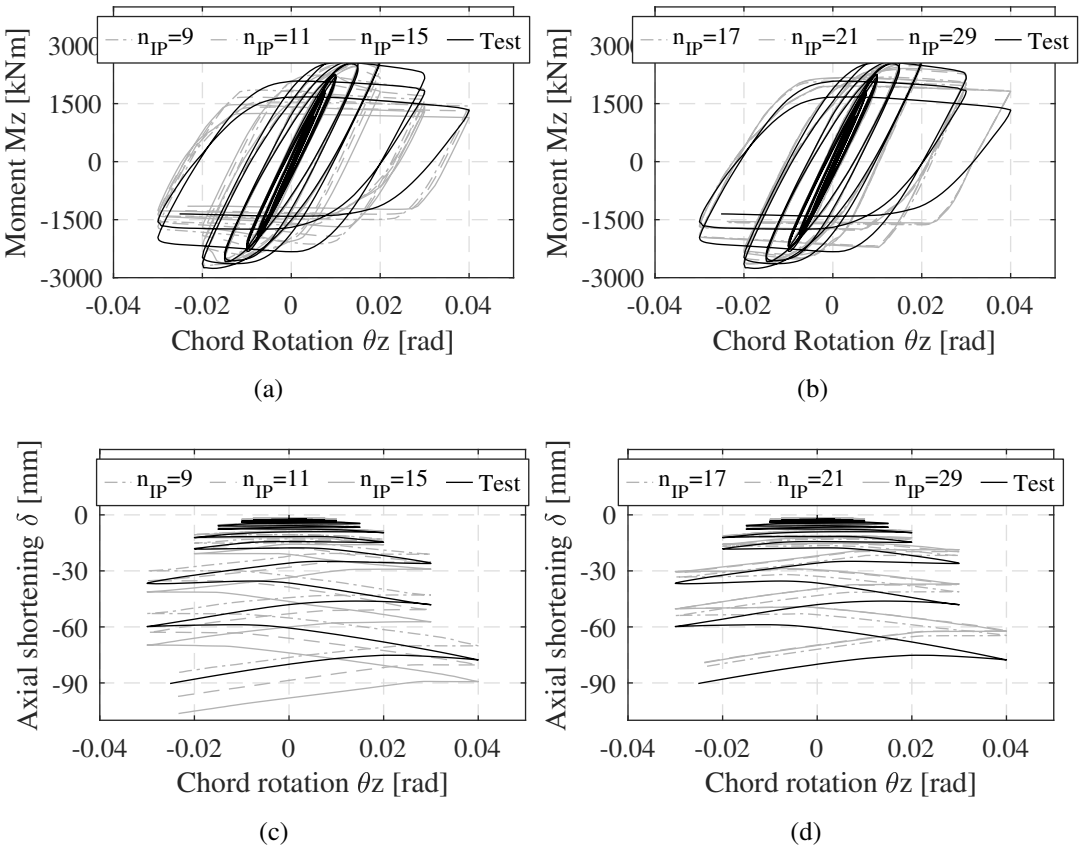

Figure 3: Model validation with steel wide flange column: (a) moment-rotation strong axis $l_c = 0$; (b) moment-rotation strong axis $l_c = 1.0d$; (c) axial shortening-rotation $l_c = 0$; and (d) axial shortening-rotation $l_c = 1.0d$ [test data from [3]]

3.2 System level

The objective of this section is to demonstrate the effectiveness of the proposed modeling approach for predicting the 3-dimensional response of steel frame structures through collapse. The discussion is based on nonlinear response history analyses of a full-scale 4-story steel frame building tested on the E-Defense shake table in Japan. The studied building was subjected to 3D shaking at increasing intensities (20%, 40%, 60%, and 100%) of the original JR Takatori record from the 1995 Kobe earthquake. The case study building, shown in Figure 4a consists of steel moment-resisting frames (MRFs) as lateral load resistance system in both directions. Further details on the case study building can be found in [24, 25]. The steel columns were cold-formed hollow square sections (HSS) made from BCR295 structural steel, while the steel beams were wide flange sections made from SN400B steel. The building lost its lateral load capacity during the unscaled JR Takatori record due to inelastic local buckling at the first-story column ends, resulting in a 'soft' first story collapse mechanism.

Figure 5 depicts the modeling approach for the 3D simulations that are conducted in a customized version of the Open System for Earthquake Engineering Simulation (OpenSees) version 3.3.0 [22]. As shown in this figure, the proposed modeling approach uses the developed force-based beam-column element with selective gradient inelasticity and the developed multiaxial material law formulation with softening for the columns. In contrast, the beams and

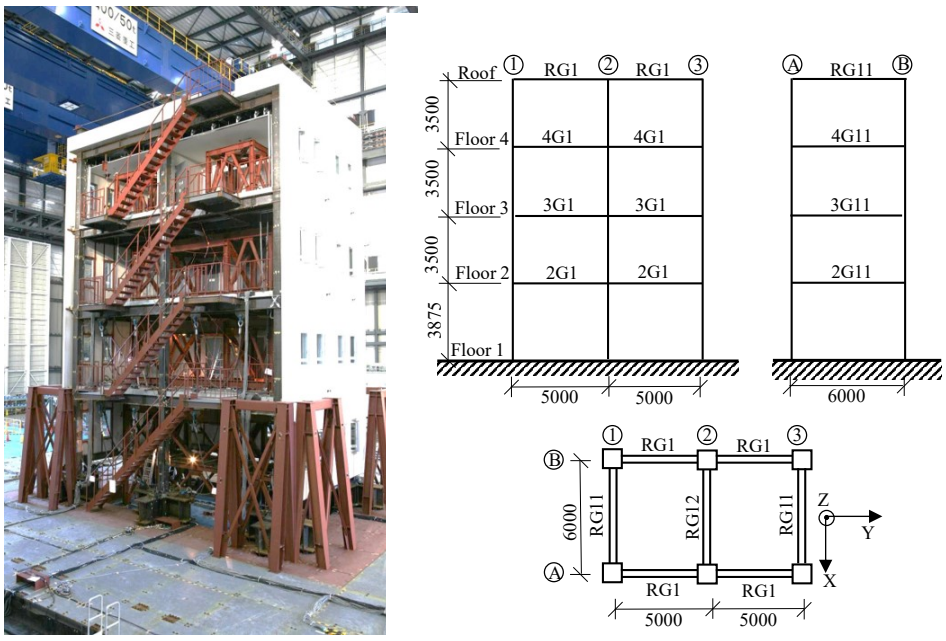

Figure 4: Case study building: (a) building overview after construction [image adopted from [25]] and (b) elevation and plan views

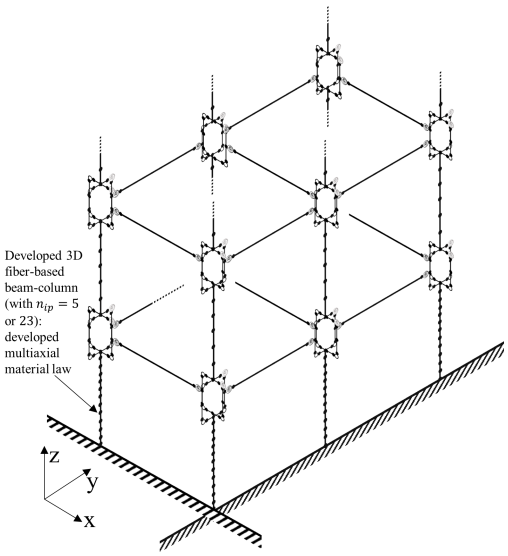

Figure 5: Modeling approach for the 3D simulations

panel zones are modeled with standard elastic beam-column elements with zero-length rotational spring according to procedures by [4, 5] for the former and [26] for the latter. Further details on the modeling approach can be found in [19].

Simulation results are compared for the unscaled JR Takatori record, focusing on the modeling approach of the first-story columns. The proposed beam-column element with selective gradient inelasticity is used in three cases: (i) a characteristic length l_c equal to the section depth is assumed for the gradient formulation, corresponding to the column buckling length [24], with 23 integration points along the element length, ensuring at least three integration sections within

l_c (denoted as '3D GI 23IP'); (ii) local formulation with 23 integration points ('3D L 23IP'); and (iii) local formulation with 5 integration points ('3D L 5IP'). In all cases, the developed multiaxial material law with softening is assigned to the section fibers, with material parameters computed as detailed in [19].

Figures 6 to 8 show selected 3D simulation results for the unscaled JR Takatori record until the building lost lateral load capacity. The first story drift ratio (SDR_1) predictions (Figure 6a) are fairly insensitive to the element formulation, and the accuracy of the predicted response is notable across all 3D models. However, this is case for the particular building that is susceptible to a first story collapse mechanism. As shown in Figure 7, the 3D simulations effectively capture the building orbit prior to the concentration of the inelastic deformations in the Y-direction once the lateral SDR exceeds 2%. Figure 8 shows that strain localization due to local buckling. This issue impacts the post-peak response of the exterior column A1. Specifically, results from the local formulation ('3D L 5IP' and '3D L 23IP' in Figure 8) reveal a steeper negative slope and accelerated strength deterioration in the softening branch when 23 integration sections are used, compared to the case with 5 integration sections.

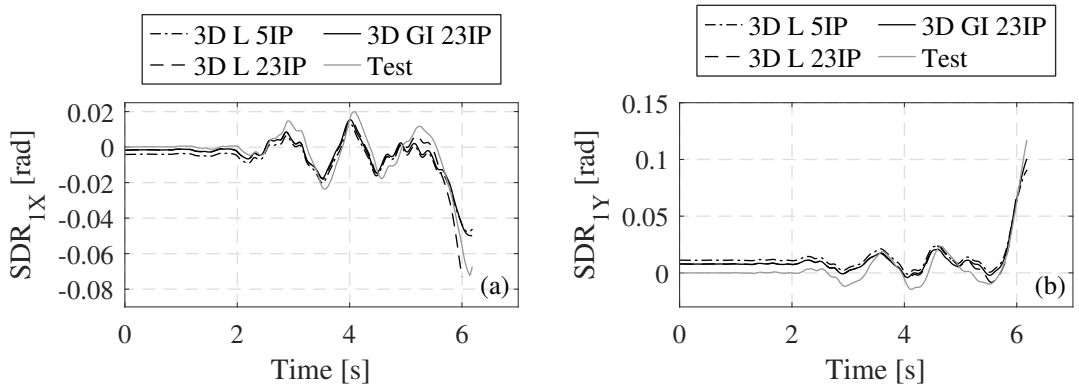

Figure 6: Comparison of first story drift ratio histories

4 SUMMARY AND CONCLUSIONS

This paper introduces new methodological developments for simulating the earthquake-induced collapse of steel frame structures under 3-dimensional earthquake loading. The approach leverages a newly developed 3D beam-column element with selective gradient-inelasticity and a multiaxial material law with softening. The material law effectively captures cyclic hardening, softening and recovery due to cyclic inelastic local buckling. The proposed element formulation ensures mesh-convergent results, addressing challenges associated with strain localization and mesh-divergence in the presence of a material law that exhibits softening. Both developed formulations are implemented in the OpenSees simulation platform and are validated through member- and system-level experiments. These comparisons demonstrate the ability of the proposed modeling approach to accurately capture the response of steel members and frame structures during strong ground motion shaking, including collapse. The results of the system-level simulations provide valuable insights into the collapse mechanisms of steel frame structures under earthquake loading by means of 3-dimensional simulations.

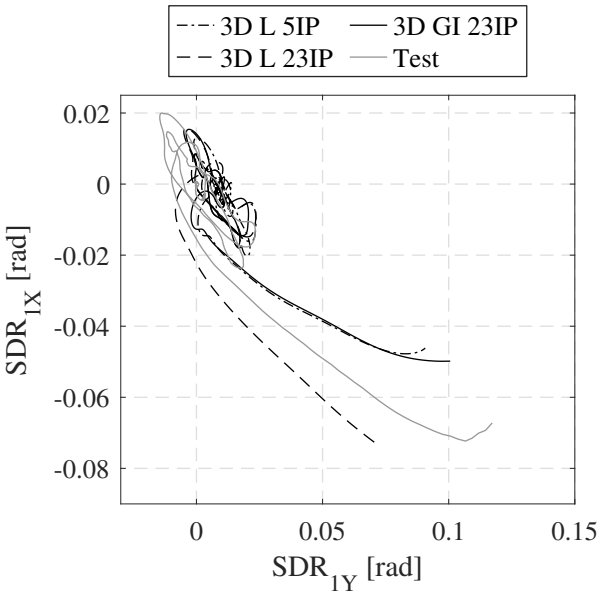

Figure 7: Comparisons of first story drift ratio orbits

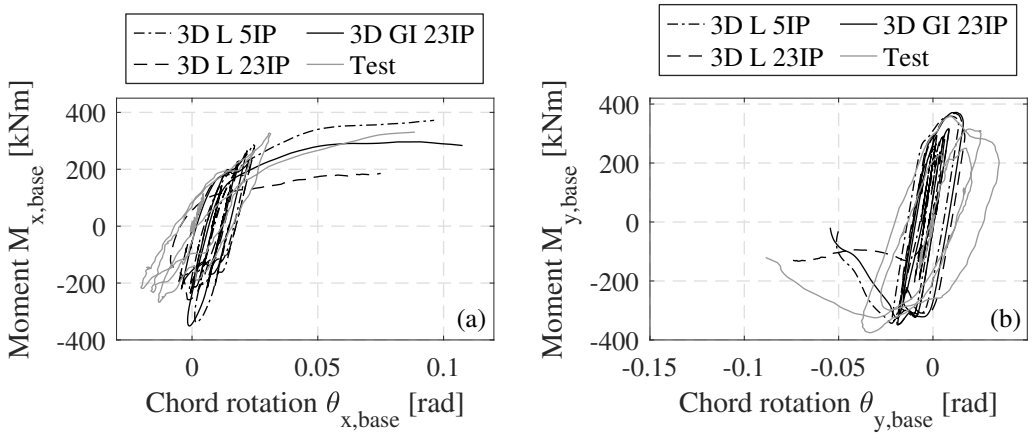

Figure 8: Comparison between predictions in moment-chord rotation relations of first story interior column A1

5 ACKNOWLEDGMENTS

This study is based on work supported by the Swiss National Science Foundation (Award Number: 200021_188476) and by an internal research grant from École Polytechnique Fédérale de Lausanne. The financial support is gratefully acknowledged. Any opinions, findings, and conclusions expressed in this paper are those of the authors and do not necessarily reflect the views of the sponsors.

References

[1] FEMA. *Seismic performance assessment of buildings, volume 1 - methodology: FEMA P-58-1*. Tech. rep. Washington DC, USA: Federal Emergency Management Agency, Dec. 2018.

[2] FEMA. *Seismic performance assessment of buildings, volume 2 - implementation guide: FEMA P-58-2*. Tech. rep. Washington DC, USA: Federal Emergency Management Agency, Dec. 2018.

[3] Ahmed Elkady and Dimitrios G. Lignos. "Full-scale testing of deep wide-flange steel columns under multiaxis cyclic loading: loading sequence, boundary effects, and lateral stability bracing force demands". In: *Journal of Structural Engineering* 144.2 (Feb. 2018), p. 04017189.

[4] Luis F. Ibarra and Helmut Krawinkler. *Global collapse of frame structures under seismic excitations*. Tech. rep. 152. The John A. Blume Earthquake Engineering Center, Departement of Civil and Environmental Engineering Stanford University, California, U.S.A., Aug. 2005.

[5] Dimitrios G. Lignos and Helmut Krawinkler. "Deterioration modeling of steel components in support of collapse prediction of steel moment frames under earthquake loading". In: *Journal of Structural Engineering* 137.11 (Nov. 2011), pp. 1291–1302.

[6] Fabio F Taucer, Enrico Spacone, and Filip C Filippou. *A fiber beam-column element for seismic response analysis of reinforced concrete structures*. Tech. rep. UCB/EERC-91/17. University of California Berkeley, California, U.S.A., 1991.

[7] E. Spacone, V. Ciampi, and F.C. Filippou. "Mixed formulation of nonlinear beam finite element". In: *Computers & Structures* 58.1 (Jan. 1996), pp. 71–83.

[8] J Coleman and Enrico Spacone. "Localization issues in force-based frame elements". In: *Journal of Structural Engineering* 127.11 (Nov. 2001), pp. 1257–1265.

[9] Michael H. Scott and Gregory L. Fenves. "Plastic hinge integration methods for force-based beam–column elements". In: *Journal of Structural Engineering* 132.2 (Feb. 2006), pp. 244–252.

[10] Diego Isidoro Heredia Rosa, Albano De Castro E Sousa, Dimitrios G. Lignos, Arka Maity, and Amit Kanvinde. "A multiaxial plasticity model with softening for simulating inelastic local buckling in steel beam columns under monotonic loading through fiber elements". In: *Journal of Structural Engineering* 151.1 (Jan. 2025), p. 04024196.

[11] Diego I. Heredia Rosa, Albano de Castro e Sousa, Dimitrios G. Lignos, Arka Maity, and Amit Kanvinde. "A multiaxial plasticity model with softening for simulating inelastic local buckling in steel beam-columns under cyclic loading through fiber elements (accepted)". In: *Journal of Structural Engineering* (2025).

[12] Veronique Le Corvec. "Nonlinear 3d frame element with multi-axial coupling under consideration of local effects". PhD thesis. Department of Civil and Environmental Engineering, University of California Berkeley: California, U.S.A., 2012.

[13] Arka Maity, Amit Kanvinde, Diego I. Heredia Rosa, Albano de Castro e Sousa, and Dimitrios G. Lignos. "A displacement-based fiber element to simulate interactive lateral torsional and local buckling in steel members". In: *Journal of Structural Engineering* 149.5 (May 2023), p. 04023045.

[14] Alexander R. Hartloper, Albano de Castro e Sousa, and Dimitrios G. Lignos. "Constitutive modeling of structural steels: nonlinear isotropic/kinematic hardening material model and its calibration". In: *Journal of Structural Engineering* 147.4 (Apr. 2021), p. 04021031.

[15] Germund Dahlquist and Ake Bjorck. *Numerical methods in scientific computing*. Philadelphia: Society for Industrial and Applied Mathematics, 2008.

[16] R.H.J. Peerlings, M.G.D. Geers, R. de Borst, and W.A.M. Brekelmans. "A critical comparison of nonlocal and gradient-enhanced softening continua". In: *International Journal of Solids and Structures* 38.44-45 (Nov. 2001), pp. 7723–7746.

[17] Julien Cravero, Ahmed Elkady, and Dimitrios G. Lignos. “Experimental evaluation and numerical modeling of wide-flange steel columns subjected to constant and variable axial load coupled with lateral drift demands”. In: *Journal of Structural Engineering* 146.3 (Mar. 2020), p. 04019222.

[18] Yusuke Suzuki and Dimitrios G. Lignos. “Experimental evaluation of steel columns under seismic hazard-consistent collapse loading protocols”. In: *Journal of Structural Engineering* 147.4 (Apr. 2021), p. 04021020.

[19] Diego I. Heredia Rosa. “A softening constitutive law and gradient-inelastic fiber-based element for 3-dimensional frame simulations under seismic excitations”. PhD thesis (advisors: Lignos, D. G. and de Castro e Sousa, A.) Department of Architecture, Civil and Environmental Engineering, Ecole Polytechnique Federale Lausanne, Switzerland, June 2024.

[20] Petros Sideris and Mohammad Salehi. “A gradient inelastic flexibility-based frame element formulation”. In: *Journal of Engineering Mechanics* 142.7 (July 2016), p. 04016039.

[21] Mohammad Salehi and Petros Sideris. “Refined gradient inelastic flexibility-based formulation for members subjected to arbitrary loading”. In: *Journal of Engineering Mechanics* 143.9 (Sept. 2017), p. 04017090.

[22] Frank McKenna. “Object-oriented finite element programming: Frameworks for analysis, algorithms and parallel computing”. PhD thesis. Department of Civil Engineering, University of California, Berkeley: California, U.S.A., 1997.

[23] Milton Abramowitz and Irene A. Stegun, eds. *Handbook of mathematical functions: with formulas, graphs, and mathematical tables*. 9. Dover books on mathematics. New York, NY: Dover Publications, 1965.

[24] Yuichi Matsuoka. “Steel structural frames with non-structural members - Shaking table experiment and seismic performance evaluation”. PhD thesis. Kyoto University, Kyoto, Japan (in Japanese), Nov. 2009.

[25] Dimitrios G. Lignos, Tsuyoshi Hikino, Yuichi Matsuoka, and Masayoshi Nakashima. “Collapse assessment of steel moment frames based on e-defense full-scale shake table collapse tests”. In: *Journal of Structural Engineering* 139.1 (Jan. 2013), pp. 120–132.

[26] Andronikos Skiadopoulos and Dimitrios G. Lignos. “Seismic demands of steel moment resisting frames with inelastic beam-to-column web panel zones”. In: *Earthquake Engineering & Structural Dynamics* 51.7 (June 2022), pp. 1591–1609.